

Experimental study of turbulent thermal diffusion of particles in an inhomogeneous forced convective turbulence

E. Elmakies, O. Shildkrot, N. Kleeorin, A. Levy, and I. Rogachevskii*

The Pearlstone Center for Aeronautical Engineering Studies, Department of Mechanical Engineering, Ben-Gurion University of the Negev, P.O.Box 653, Beer-Sheva 8410530, Israel

(Dated: June 21, 2023)

We investigate experimentally phenomenon of turbulent thermal diffusion of micron-size solid particles in an inhomogeneous convective turbulence forced by one vertically-oriented oscillating grid in an air flow. This effect causes formation of large-scale inhomogeneities in particle spatial distributions in a temperature-stratified turbulence. We perform detailed comparisons of the experimental results with those obtained in our previous experiments with an inhomogeneous and anisotropic stably stratified turbulence produced by a one oscillating grid in the air flow. Since the buoyancy increases the turbulent kinetic energy for convective turbulence and decreases it for stably stratified turbulence, the measured turbulent velocities for convective turbulence are larger than those for stably stratified turbulence. This tendency is also seen in the measured vertical integral turbulent length scales. Measurements of temperature and particle number density spatial distributions show that particles are accumulated in the vicinity of the minimum of the mean temperature due to phenomenon of turbulent thermal diffusion. This effect is observed in both, convective and stably stratified turbulence, where we find the effective turbulent thermal diffusion coefficient for micron-size particles. The obtained experimental results are in agreement with theoretical predictions.

I. INTRODUCTION

Turbulent transport of particles has been a subject of many studies due to numerous applications in geophysics and environmental sciences, astrophysics, and various industrial flows [1–7]. Different mechanisms of large-scale and small-scale clustering of inertial particles have been proposed. The large-scale clustering occurs in scales which are much larger than the integral scale of turbulence, while the small-scale clustering is observed in scales which are much smaller than the integral turbulence scale.

The large-scale clustering of inertial particles in isothermal non-stratified inhomogeneous turbulence occurs due to turbophoresis [8–13], which is a combined effect of particle inertia and inhomogeneity of turbulence. Turbophoresis results in appearance of the additional non-diffusive turbulent flux of inertial particles $\mathbf{J}_{\text{turboph}} = \bar{n} \bar{\mathbf{V}}_{\text{turboph}}$, where the mean particle velocity caused by turbophoresis can be written as

$$\bar{\mathbf{V}}_{\text{turboph}} = -\kappa_{\text{turb}} \frac{\nabla \langle \mathbf{u}^2 \rangle}{2}. \quad (1)$$

Here \bar{n} is the mean number density of inertial particles, \mathbf{u} is the turbulent fluid velocity, κ_{turb} is the turbophoretic coefficient which generally depends on the Stokes number $St = \tau_p/\tau_\nu$ and the fluid Reynolds number $Re = \ell_0 u_{\text{rms}}/\nu$, where $\tau_\nu = \tau_0/Re^{1/2}$ is the Kolmogorov viscous time, $\tau_0 = \ell_0/u_{\text{rms}}$ is the characteristic turbulent time, ν is the kinematic viscosity, $u_{\text{rms}} \equiv \sqrt{\langle \mathbf{u}^2 \rangle}$ is the rms velocity in the integral turbulence scale ℓ_0 and τ_p is

the Stokes time for the small spherical particles. Due to turbophoresis, inertial particles are accumulated in the vicinity of the minimum of the turbulent intensity. In particular, direct numerical simulations (DNS) [13] show that inertial particles in inhomogeneously forced isothermal turbulent flows are accumulated at the minima of turbulent velocity. Two turbulent transport processes, turbophoresis and turbulent diffusion determine the spatial distribution of the particles. Numerical simulations [13] demonstrate that the non-dimensional product of the turbophoretic coefficient κ_{turb} and the rms velocity u_{rms} increases linearly with the parameter St_f for $St_f \ll 1$, reaches a maxima for $St_f \sim 10$ and decreases as $St_f^{-1/3}$ for large St_f , where $St_f = \tau_p/\tau_0$ is the Stokes number defined using the characteristic flow time scale τ_0 based on the forcing scale of turbulence. The same large-scale clustering phenomenon caused by turbophoresis has been studied in DNS of turbulent Kolmogorov flows [14]. Although the authors do not interpret their results as a balance between turbophoretic and turbulent diffusive fluxes, they do observe that the large-scale clustering increases for small St_f but this trend reverses smoothly at higher values of St_f . The large-scale clustering due to turbophoresis has been also observed in DNS of turbulent channel flows [15] and in various experimental studies [16, 17].

Another example of the large-scale clustering of inertial particles is the phenomenon of turbulent thermal diffusion that is a combined effect of the temperature stratified turbulence and inertia of small particles [18, 19]. Turbulent thermal diffusion is a purely collective phenomenon occurring in temperature stratified turbulence and resulting in the appearance of a non-zero mean effective velocity of particles in the direction opposite to the mean temperature gradient. This implies that this phenomenon causes a non-diffusive turbulent flux of particles

* gary@bgu.ac.il

in the direction of the turbulent heat flux. A competition between the turbulent thermal diffusion and turbulent diffusion determines the conditions for the formation of large-scale particle concentrations in the vicinity of the mean temperature minimum.

Turbulent thermal diffusion has been intensively investigated analytically [18–25] using different theoretical approaches. This effect has been detected in DNS [26, 27]. Turbulent thermal diffusion has been observed in geophysical turbulence, e.g., in the atmosphere of the Earth [28] and the atmosphere of Titan [29], and it also has been discussed in astrophysical turbulence applications [30]. Moreover, the phenomenon of turbulent thermal diffusion has been detected in laboratory experiments in nearly isotropic and homogeneous turbulence produced by two oscillating grids [25, 31–33] and in a multi-fan produced turbulence [34]. Recently the phenomenon of turbulent thermal diffusion has been found in an inhomogeneous and anisotropic stably stratified turbulence produced by one oscillating grid in the air flow [35]. These experiments have demonstrated formation of inhomogeneous distributions of micron-size particles in the vicinity of the mean temperature minimum.

The main goal of the present study is to investigate experimentally the phenomenon of turbulent thermal diffusion of the micron-size solid particles in an inhomogeneous convective turbulence forced by one oscillating grid in the air flow. In the experiments, we measure velocity fields applying Particle Image Velocimetry (PIV). We measure temperature field with a temperature probe equipped with 12 E thermocouples. In addition, we determine spatial distributions of small solid particles by a PIV system using the effect of the Mie light scattering by particles in the flow. We perform detailed comparisons of the obtained experimental results with those in the experiments in an inhomogeneous and anisotropic stably stratified turbulence produced by one oscillating grid [35] and in a convective turbulence forced by two oscillating grids in the air flow [36]. This paper is organized as follows. In Sec. II we elucidate the mechanism of the phenomenon of turbulent thermal diffusion and determine the turbulent flux of particles using the spectral τ approach for fully developed temperature-stratified turbulence. In Sec. III we discuss our experimental facilities and instrumentation, and in Sec. IV we describe the obtained experimental results. Finally, in Sec. V we outline conclusions.

II. TURBULENT THERMAL DIFFUSION

In this section we determine the turbulent flux of particles in a temperature-stratified turbulence and elucidate the mechanism related to the effect of turbulent thermal diffusion. We study dynamics of small non-inertial particles advected by a turbulent fluid flow. An evolution of the particle number density $n(t, \mathbf{x})$ in a fluid velocity field $\mathbf{U}(t, \mathbf{x})$ is determined by the convective-diffusion

equation:

$$\frac{\partial n}{\partial t} + \nabla \cdot (n \mathbf{U} - D \nabla n) = 0, \quad (2)$$

where $D = k_B T / (6\pi\rho\nu a_p)$ is the coefficient of the molecular (Brownian) diffusion of particles having the radius a_p . Here T and ρ are the fluid temperature and density, respectively and k_B is the Boltzmann constant. The fluid velocity is a turbulent field produced by, e.g., an external steering force. Equation (2) is a conservation law for the total number of particles that implies that the total number of particles is conserved in a closed volume. Here we do not consider a coagulation of particles or chemical reactions as well as condensation or evaporation of droplets which change the total number of particles or droplets in a closed volume.

Assuming for simplicity, that the diffusion coefficient is independent of coordinates, Eq. (2) can be rewritten as

$$\frac{\partial n}{\partial t} + \nabla \cdot (n \mathbf{U}) = D \Delta n. \quad (3)$$

We use a point-particle approximation that implies that the size of particles is very small in comparison with all possible scales of fluid motions. When the fluid velocity is much less than the sound speed (i.e., for low-Mach-number fluid flows), the continuity equation for the fluid density can be used in an anelastic approximation, $\nabla \cdot (\rho \mathbf{U}) = 0$. This equation can be rewritten as $\nabla \cdot \mathbf{U} = -(\mathbf{U} \cdot \nabla) \ln \rho$, i.e., the anelastic approximation takes into account an inhomogeneous fluid density.

We study a long-term evolution of the particle number density in spatial scales L_n which are much larger than the integral scale of turbulence ℓ_0 , and during the time scales t_n which are much larger than the turbulent time scales τ_0 . We use a mean-field approach in which all quantities are decomposed into the mean and fluctuating parts, where the fluctuating parts have zero mean values, i.e., we use the Reynolds averaging. In particular, the particle number density $n = \bar{n} + n'$, where $\bar{n} = \langle n \rangle$ is the mean particle number density, and n' are particle number density fluctuations and $\langle n' \rangle = 0$. The angular brackets $\langle \dots \rangle$ denote an ensemble averaging. Averaging Eq. (3) over an ensemble of a turbulent velocity field, we arrive at the mean-field equation for the particle number density:

$$\frac{\partial \bar{n}}{\partial t} + \nabla \cdot (\bar{\mathbf{U}} \bar{n} + \langle \mathbf{u} n' \rangle) = D \Delta \bar{n}, \quad (4)$$

where $\mathbf{F} \equiv \langle \mathbf{u} n' \rangle$ is the turbulent flux of particles. We consider for simplicity the case $\bar{\mathbf{U}} = 0$.

To derive an expression for the turbulent flux of particles, we obtain the equation for particle number density fluctuations n' , by subtracting Eq. (4) from Eq. (3), which yields

$$\frac{\partial n'}{\partial t} = -\tilde{Q} - (\mathbf{u} \cdot \nabla) \bar{n} - \bar{n} (\nabla \cdot \mathbf{u}) + D \Delta n', \quad (5)$$

where $\tilde{\mathcal{Q}} = \nabla \cdot (n' \mathbf{u} - \langle n' \mathbf{u} \rangle)$ is the nonlinear term. The source term for particle number density fluctuations, $-(\mathbf{u} \cdot \nabla) \bar{n}$, results in a production of particle number density fluctuations by the tangling of the gradient $\nabla \bar{n}$ of the mean particle number density by velocity fluctuations. The other source term, $-\bar{n}(\nabla \cdot \mathbf{u})$ for particle number density fluctuations can be rewritten as $-\bar{n}(\nabla \cdot \mathbf{u}) = (\bar{n}/\bar{\rho})(\mathbf{u} \cdot \nabla) \bar{\rho}$, where we take into account the anelastic approximation, $\nabla \cdot \mathbf{u} = -(1/\bar{\rho})(\mathbf{u} \cdot \nabla) \bar{\rho}$, which is also valid for the mean fluid density, $\bar{\rho}$. This implies that this source term describes a production of particle number density fluctuations by the tangling of the gradient $\nabla \bar{\rho}$ of the mean fluid density by velocity fluctuations. We use the Péclet number $\text{Pe} = |\tilde{\mathcal{Q}}|/|D\Delta n'|$ defined as the dimensionless ratio of the absolute values of the nonlinear term $|\tilde{\mathcal{Q}}|$ to the diffusion term $|D\Delta n'|$. The Péclet number can be estimated as $\text{Pe} = \ell_0 u_{\text{rms}}/D$. We consider the case of large Péclet and Reynolds number. Since the nonlinear equation (5) cannot be solved exactly for arbitrary Péclet numbers, we consider the case of large Péclet and Reynolds numbers, which corresponds to our laboratory experiments.

We apply the Fourier transform only in a \mathbf{k} space but not in a ω space, because in a fully developed Kolmogorov-like turbulence, the turbulent time is universally related to spatial scales. We take into account the nonlinear terms in equations for velocity and particle number density fluctuations and apply the spectral τ approach [37, 38] (see also Ref. [7] for detail discussion).

For simplicity, we consider a one-way coupling by taking into account the effect of turbulence on the particle number density, and neglecting the feedback effect of the particle number density on the turbulent fluid flow. The one-way coupling approximation is valid when the spatial density of particles $n m_p$ is much smaller than the fluid density ρ , where m_p is the particle mass. First, we consider non-inertial particles, which means that the particles move with the fluid velocity, i.e., the particle number density is a passive scalar.

We use a multi-scale approach [39], i.e., we consider the one-point second-order correlation function as:

$$\begin{aligned} \langle u_i(t, \mathbf{x}) n'(t, \mathbf{x}) \rangle &\equiv \lim_{\mathbf{x} \rightarrow \mathbf{y}} \langle u_i(t, \mathbf{x}) n'(t, \mathbf{y}) \rangle \\ &= \lim_{\mathbf{r} \rightarrow 0} \int F_i(t, \mathbf{k}, \mathbf{R}) \exp(i \mathbf{k} \cdot \mathbf{r}) d\mathbf{k} = \int F_i(t, \mathbf{k}, \mathbf{R}) d\mathbf{k}, \end{aligned} \quad (6)$$

where $F_i(t, \mathbf{k}, \mathbf{R}) = \int F_i(t, \mathbf{k}, \mathbf{K}) \exp(i \mathbf{K} \cdot \mathbf{R}) d\mathbf{K}$ and $F_i(t, \mathbf{k}, \mathbf{K}) = \langle u_i(t, \mathbf{k} + \mathbf{K}/2) n'(t, -\mathbf{k} + \mathbf{K}/2) \rangle$. Here the mean fields depend on “slow” variables $\mathbf{R} = (\mathbf{x} + \mathbf{y})/2$, while fluctuations depend on “fast” variables $\mathbf{r} = \mathbf{x} - \mathbf{y}$, which correspond to large-scale and small-scale spatial variables, respectively. In the Fourier space, $\mathbf{k} = (\mathbf{k}_1 - \mathbf{k}_2)/2$, corresponds to the small scales, and $\mathbf{K} = \mathbf{k}_1 + \mathbf{k}_2$ characterizes the large scales, where we use the Fourier transform, $u_i(t, \mathbf{x}) = \int u_i(t, \mathbf{k}_1) \exp(i \mathbf{k}_1 \cdot \mathbf{x}) d\mathbf{k}_1$. For homogeneous turbulence, the correlation function, $F_i(t, \mathbf{k}, \mathbf{R})$ is independent of the large-scale variable \mathbf{R} ,

i.e., $F_i(t, \mathbf{k}, \mathbf{R}) = F_i(t, \mathbf{k})$.

To obtain expression for the particle turbulent flux, we use Eq. (5) written in a Fourier space. This allows us to derive equation for the correlation function $F_j(t, \mathbf{k})$ in a Fourier space as

$$\frac{\partial F_j(\mathbf{k})}{\partial t} = -(\nabla_i \bar{n} - i k_i \bar{n}) f_{ij}(-\mathbf{k}) + \hat{\mathcal{M}} F_j^{(III)}(\mathbf{k}), \quad (7)$$

where for the brevity of notation, hereafter we omit argument t in the correlation functions. Here $\hat{\mathcal{M}} F_i^{(III)}(\mathbf{k}) = \langle [\partial u_i(t, \mathbf{k})/\partial t] n'(t, -\mathbf{k}) \rangle - \langle u_i(t, \mathbf{k}) \mathcal{Q}(t, -\mathbf{k}) \rangle$ are the third-order moments appearing due to the nonlinear terms $\tilde{\mathcal{Q}}$ in Eq. (5) and the nonlinear Navier-Stokes equation. Here $f_{ij}(\mathbf{k}) = \langle u_i(t, \mathbf{k}) u_j(t, -\mathbf{k}) \rangle$ and $\mathcal{Q} = \tilde{\mathcal{Q}} - D\Delta n'$.

We use the spectral τ approximation [37, 38]. This approximation postulates that the deviations of the third-moment terms, $\hat{\mathcal{M}} F^{(III)}(\mathbf{k})$, from the contributions to these terms afforded by the background turbulence, $\hat{\mathcal{M}} F^{(III,0)}(\mathbf{k})$, can be expressed through the similar deviations of the second moments, $F(\mathbf{k}) - F^{(0)}(\mathbf{k})$:

$$\hat{\mathcal{M}} F^{(III)}(\mathbf{k}) - \hat{\mathcal{M}} F^{(III,0)}(\mathbf{k}) = -\frac{1}{\tau_r(k)} \left[F(\mathbf{k}) - F^{(0)}(\mathbf{k}) \right], \quad (8)$$

where $\tau_r(k)$ is the scale-dependent relaxation time, which can be identified with the correlation time $\tau(k)$ of the turbulent velocity field for large Reynolds and Péclet numbers. The functions with the superscript (0) correspond to the background turbulence with a zero turbulent particle flux and a zero level of particle number density fluctuations. Consequently, Eq. (8) reduces to $\hat{\mathcal{M}} F_i^{(III)}(\mathbf{k}) = -F_i(\mathbf{k})/\tau(k)$. Validation of the τ approximation for different situations has been performed in various numerical simulations [26, 27, 40–44] (see also Ref. [7] for detail discussion of the ranges of applicability of this approach).

We assume that the characteristic time of variation of the second moment $F_i(\mathbf{k})$ is substantially larger than the correlation time $\tau(k)$ for all turbulence scales. This allows us to use a steady-state solution of Eq. (7). Applying the spectral τ approximation and using the steady-state solution of Eq. (7), we obtain the following formula for the turbulent flux of particles, $F_j(\mathbf{k})$ as

$$F_j(\mathbf{k}) = -\tau(k) (\nabla_i \bar{n} - i k_i \bar{n}) f_{ij}^{(0)}(-\mathbf{k}), \quad (9)$$

where since we consider a one-way coupling, we replace the function $f_{ij}(\mathbf{k})$ by $f_{ij}^{(0)}(\mathbf{k})$ in Eq. (9).

We use the following model for the second moments of turbulent velocity field $f_{ij}^{(0)}(\mathbf{k}) \equiv \langle u_i(\mathbf{k}) u_j(-\mathbf{k}) \rangle^{(0)}$ of an isotropic and homogeneous background turbulence in anelastic approximation in a Fourier space:

$$f_{ij}^{(0)}(\mathbf{k}) = \frac{\langle \mathbf{u}^2 \rangle E(k)}{8\pi k^2} \left[\delta_{ij} - k_{ij} + \frac{i}{k^2} (\lambda_i k_j - \lambda_j k_i) \right],$$

(10)

where $k_{ij} = k_i k_j / k^2$, δ_{ij} is the Kronecker unit tensor, $\boldsymbol{\lambda} = -(\nabla \bar{\rho}) / \bar{\rho}$, the spectrum function of the turbulent kinetic energy density is $E(k) = (2/3) k_0^{-1} (k/k_0)^{-5/3}$ [see Ref. [7] for detail derivation of Eq. (10)]. Here the wavenumber k varies within the interval $k_0 \leq k \leq k_\nu$ corresponding to the inertial range of scales, the wave number $k_0 = 1/\ell_0$, the length ℓ_0 is the integral scale of turbulence, the wave number $k_\nu = \ell_\nu^{-1}$, where $\ell_\nu = \ell_0 \text{Re}^{-3/4}$ is the Kolmogorov (viscous) scale and the turbulent correlation time is given by $\tau(k) = 2\tau_0 (k/k_0)^{-2/3}$, where τ_0 is the characteristic turbulent time. The functions $E(k)$ and $\tau(k)$ correspond to fully developed turbulence with the Kolmogorov scalings.

Substituting Eq. (10) into Eq. (6), we determine the turbulent flux of particles $F_i = \langle u_i n' \rangle$:

$$F_i = -\frac{\langle \mathbf{u}^2 \rangle}{8\pi} \int_{k_0}^{k_\nu} \tau(k) E(k) dk \int_0^{2\pi} d\varphi \int_0^\pi \sin \vartheta d\vartheta \times [(\delta_{ij} - k_{ij}) \nabla_i \bar{n} + (\lambda_j - \lambda_i k_{ij}) \bar{n}]. \quad (11)$$

For the integration over \mathbf{k} in Eq. (11), we use the integrals given by $\int_0^{2\pi} d\varphi \int_0^\pi \sin \vartheta d\vartheta k_{ij} = (4\pi/3) \delta_{ij}$ and $\int_{k_0}^{k_\nu} \tau(k) E(k) dk = \tau_0$. After integration over \mathbf{k} , we obtain the particle turbulent flux $\langle n' \mathbf{u} \rangle$ as

$$\langle n' \mathbf{u} \rangle = \mathbf{V}^{\text{eff}} \bar{n} - D_T \nabla \bar{n}, \quad (12)$$

where the turbulent diffusion coefficient is

$$D_T = \frac{1}{3} \tau_0 \langle \mathbf{u}^2 \rangle, \quad (13)$$

and the effective pumping velocity is given by

$$\mathbf{V}^{\text{eff}} = -D_T \boldsymbol{\lambda} = D_T \frac{\nabla \bar{\rho}}{\bar{\rho}}. \quad (14)$$

Equations (12)–(14) are in agreement with those obtained using dimensional analysis (see Ref. [7] for detail discussions). Note that the phenomenon of turbulent diffusion of particles has been predicted about 100 years ago in Ref. [45].

To understand the mechanism related to the effective pumping velocity \mathbf{V}^{eff} , we use the equation of state for a perfect gas,

$$P = \frac{k_B}{m_\mu} \rho T \equiv \frac{R}{\mu} \rho T, \quad (15)$$

where P is the fluid pressure, $k_B = R/N_A$ is the Boltzmann constant, R is the gas constant, N_A is the Avogadro number, $\mu = m_\mu N_A$ is the molar mass, and m_μ is the molecule mass. We rewrite the equation of state for the mean fields assuming that $\bar{\rho} \bar{T} \gg \langle \rho' \theta \rangle$, where ρ' and θ are fluctuations of the fluid density and temperature, respectively, and \bar{T} is the mean fluid temperature. Thus, the equation of state for the mean fields reads:

$$\bar{P} = \frac{k_B}{m_\mu} \bar{\rho} \bar{T}, \quad (16)$$

where \bar{P} is the mean pressure.

Using Eq. (16), we express the gradient of the mean fluid density in terms of the gradients of the mean fluid pressure $\nabla \bar{P}$ and mean fluid temperature $\nabla \bar{T}$ as

$$\frac{\nabla \bar{\rho}}{\bar{\rho}} = \frac{\nabla \bar{P}}{\bar{P}} - \frac{\nabla \bar{T}}{\bar{T}}. \quad (17)$$

Substituting Eq. (17) into Eq. (14), we obtain the final expression for the effective pumping velocity of non-inertial particles as

$$\mathbf{V}^{\text{eff}} = D_T \left(\frac{\nabla \bar{P}}{\bar{P}} - \frac{\nabla \bar{T}}{\bar{T}} \right). \quad (18)$$

To understand different terms in Eq. (18), we compare the molecular and turbulent fluxes of particles (or gaseous admixtures). Equation for the number density of particles reads

$$\frac{\partial n}{\partial t} + \nabla \cdot (n \mathbf{U}) = -\nabla \cdot \mathbf{F}_M, \quad (19)$$

where the molecular flux of particles \mathbf{F}_M is given by

$$\mathbf{F}_M = -D \left(\nabla n + k_t \frac{\nabla T}{T} + k_p \frac{\nabla P}{P} \right), \quad (20)$$

which comprises three terms: molecular diffusion ($\propto \nabla n$), molecular thermal diffusion for gases or thermophoresis for particles ($\propto k_t \nabla T$), and molecular barodiffusion ($\propto k_p \nabla P$), where k_t is the molecular thermal diffusion ratio and k_p is the molecular barodiffusion ratio. Note that the phenomenon of molecular thermal diffusion in gases has been predicted long ago in Refs. [46–48].

In turbulent flows, the turbulent flux of particles can be rewritten as

$$\mathbf{F}_T \equiv \langle n' \mathbf{u} \rangle = -D_T \left(\nabla \bar{n} + \bar{n} \frac{\nabla \bar{T}}{\bar{T}} - \bar{n} \frac{\nabla \bar{P}}{\bar{P}} \right), \quad (21)$$

which is obtained by substitution of Eq. (18) to Eq. (12). Comparing the molecular flux of particles (20) and the turbulent flux of particles (21), we can interpret the new additional turbulent fluxes as fluxes caused by the effects of turbulent thermal diffusion [$\propto k_T (\nabla \bar{T}) / \bar{T}$] and turbulent barodiffusion [$\propto k_P (\nabla \bar{P}) / \bar{P}$], where

$$\mathbf{F}_T \equiv \langle n' \mathbf{u} \rangle = -D_T \left(\nabla \bar{n} + k_T \frac{\nabla \bar{T}}{\bar{T}} + k_P \frac{\nabla \bar{P}}{\bar{P}} \right), \quad (22)$$

and $k_T = \bar{n}$ is the turbulent thermal diffusion ratio and $k_P = -\bar{n}$ is the turbulent barodiffusion ratio. These phenomena have been predicted in Refs. [18, 19].

For small inertial particles, the expression for the effective pumping velocity reads [11] (see also Ref. [7] for detail derivation):

$$\mathbf{V}^{\text{eff}} = -\alpha D_T \nabla \ln \bar{T}, \quad (23)$$

where

$$\alpha = 1 + 2 \frac{m_p}{m_\mu} \left(\frac{\ln \text{Re}}{\text{Pe}} \right) \frac{\bar{T}}{\bar{T}_*} = 1 + 2 \frac{V_g L_P \ln \text{Re}}{u_0 \ell_0}, \quad (24)$$

where $\tau_p V_T^2 = \gamma (m_p/m_\mu) D = \gamma V_g L_P \bar{T}_*/\bar{T}$. Here $\gamma = c_p/c_v$ is the ratio of specific heats, $V_T = (\gamma k_B \bar{T}_*/m_\mu)^{1/2}$ is the thermal velocity, \bar{T}_* is the characteristic mean fluid temperature, and $L_P = |\nabla_z \bar{P}/\bar{P}|^{-1}$ is the pressure height scale. In derivation of Eq. (24), we take into account that the Stokes time can be written as $\tau_p = \bar{\rho} V_g L_P/\bar{P}$ with $\mathbf{V}_g = \tau_p \mathbf{g}$ being the terminal fall velocity of particles, where \mathbf{g} is the acceleration caused by the gravity field. For large Péclet numbers, $\text{Pe} \gg 1$, the turbulent thermal diffusion coefficient $\alpha = 1$ for non-inertial particles, while for inertial particles α depends on the particle mass, the Reynolds and Péclet numbers.

The non-diffusive turbulent flux of particles, $\bar{n} \mathbf{V}^{\text{eff}}$, toward the mean temperature minimum is the main reason for the formation of large-scale inhomogeneous distributions of inertial particles in temperature-stratified turbulence. The steady-state solution of the equation for the mean number density of inertial particles,

$$\frac{\partial \bar{n}}{\partial t} + \nabla \cdot [\bar{n} (\mathbf{V}_g + \mathbf{V}^{\text{eff}}) - (D + D_T) \nabla \bar{n}] = 0, \quad (25)$$

satisfying the boundary condition with a zero total particle flux at the boundary, is given by

$$\frac{\bar{n}}{\bar{n}_b} = \left(\frac{\bar{T}}{\bar{T}_b} \right)^{-\frac{\alpha D_T}{D + D_T}} \exp \left[- \int_{z_b}^z \frac{V_g}{D + D_T} dz' \right], \quad (26)$$

where the subscripts (b) represent the values of the mean temperature and the mean particle number density at the boundary $z = z_b$. Equation (26) implies that small inertial particles are accumulated below the mean temperature minimum due to the gravity field.

The mechanism for turbulent thermal diffusion for inertial particles is as following. Particles inside the turbulent eddies due to its inertia tend to be drift out to the boundary regions between the eddies due to the centrifugal inertial force. Indeed, for large Péclet numbers, molecular diffusion of particles in equation for the number density of inertial particles,

$$\frac{\partial n}{\partial t} + \nabla \cdot (n \mathbf{u}^{(p)} - D \nabla n) = 0, \quad (27)$$

can be neglected, so that

$$\nabla \cdot \mathbf{u}^{(p)} \approx -n^{-1} \left[\frac{\partial n}{\partial t} + (\mathbf{u}^{(p)} \cdot \nabla) n \right] \equiv -n^{-1} \frac{dn}{dt}, \quad (28)$$

where $\mathbf{u}^{(p)}$ is the particle velocity. On the other hand, for inertial particles, $\nabla \cdot \mathbf{u}^{(p)} = \nabla \cdot \mathbf{u} + (\tau_p/\bar{\rho}) \nabla^2 p$. Indeed, the solution of the equation of motion for inertial

particles,

$$\frac{d\mathbf{u}^{(p)}}{dt} = -\frac{\mathbf{u}^{(p)} - \mathbf{u}}{\tau_p} + \mathbf{g}, \quad (29)$$

for $\rho_p \gg \bar{\rho}$ and small Stokes time, reads [49]: $\mathbf{u}^{(p)} = \mathbf{u} - \tau_p (d\mathbf{u}/dt) + \tau_p \mathbf{g} + O(\tau_p^2) \approx \mathbf{u} + \tau_p (\nabla p/\bar{\rho}) + \tau_p \mathbf{g} + O(\tau_p^2)$. Here ρ_p is the material density of particles. This yields the equation for $\nabla \cdot \mathbf{u}^{(p)}$. Therefore, in regions with maximum fluid pressure fluctuations (where $\nabla^2 p < 0$), there is accumulation of inertial particles, i.e., $dn'/dt \propto -\bar{n} (\tau_p/\bar{\rho}) \nabla^2 p > 0$. These regions obey low vorticity and high strain rate. Similarly, there is an outflow of inertial particles from regions with minimum fluid pressure.

In a homogeneous and isotropic turbulence with a zero gradient of the mean temperature, there is no a preferential direction. This implies that in a homogeneous and isotropic turbulence there is no large-scale effect of particle accumulation, and the pressure (temperature) of the surrounding fluid is not correlated with the turbulent velocity field. The only non-zero correlation is $\langle (\mathbf{u} \cdot \nabla) p \rangle$, which contributes to the flux of the turbulent kinetic energy density.

In a temperature-stratified turbulence, the turbulent heat flux does not vanish, so that fluctuations of fluid temperature θ and velocity \mathbf{u} are correlated, i.e., $\langle \theta \mathbf{u} \rangle \neq \mathbf{0}$. Fluctuations of temperature result in pressure fluctuations, which cause fluctuations of the particle number density. Increase of the pressure of the surrounding fluid is accompanied by an accumulation of particles, and the direction of the turbulent flux of particles coincides with that of the turbulent heat flux. The turbulent flux of particles is directed toward the minimum of the mean temperature. This causes the formation of large-scale inhomogeneous structures in the spatial distribution of inertial particles in the vicinity of the mean temperature minimum. In the next sections we will study this phenomenon in the experiments with a forced convective turbulence.

III. EXPERIMENTAL SETUP

In this section we describe the experimental set-up and measurement technique. We investigate turbulent thermal diffusion of small solid particles in experiments with a convective turbulence forced by one oscillating grid in the air flow. We conduct experiments in rectangular transparent chamber with dimensions $L_x \times L_y \times L_z$ with $L_x = L_z = 26$ cm and $L_y = 53$ cm, where Z is along the vertical direction and Y is perpendicular to the grid plain. The oscillating grid with bars arranged in a square array is parallel to the side walls of the chamber, it is positioned at a distance of two grid meshes from the left side wall of the chamber (see Fig. 1).

Two aluminium heat exchangers with rectangular pins $3 \times 3 \times 15$ mm are attached to the bottom (heated) and top (cooled) walls of the chamber, which allow one to

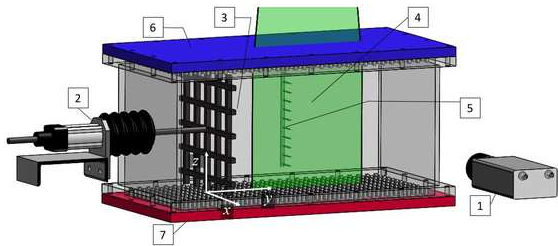


FIG. 1. Experimental setup with the forced convective turbulence: (1) digital CCD camera; (2) rod driven by the speed-controlled motor; (3) oscillating grid; (4) laser light sheet; (5) temperature probe equipped with 12 E - thermocouples; (6) heat exchanger at the top cooled wall of the chamber; (7) heat exchanger at the bottom heated wall of the chamber.

form a large vertical mean temperature gradient up to 1.8 K/cm in the main fluid flow and about 7 K/cm close to the walls. We measure the temperature field using a temperature probe equipped with 12 E - thermocouples. The thermocouples with the diameter of 0.13 mm and the sensitivity of $\approx 75 \mu\text{V/K}$ are attached to a vertical rod with a diameter 4 mm, and the mean distance between thermocouples is about 21.6 mm (see for details Ref. [35]). We measure the temperature field in many locations. The data are recorded using the developed software based on LabView 7.0, and the temperature maps are obtained using Matlab 9.7.0.

We measure the velocity field with a Particle Image Velocimetry (PIV) system [50–52], consisting in a Nd-YAG laser (Continuum Surelite 2×170 mJ) and a progressive-scan 12 bit digital CCD camera (with pixel size $6.45 \mu\text{m} \times 6.45 \mu\text{m}$ and 1376×1040 pixels). As a tracer for the PIV measurements, we use an incense smoke with spherical solid particles having the mean diameter of $0.7 \mu\text{m}$ and the material density $\rho_p \approx 10^3 \rho$. The particles are produced by high temperature sublimation of solid incense grains (see for details Ref. [35]).

For instance, the velocity fields in our experiments have been measured in a flow domain $209.09 \times 155.43 \text{ mm}^2$ with a spatial resolution of 1376×1024 pixels, so that a spatial resolution $151 \mu\text{m}$ /pixel have been achieved. We analyse the velocity field in the probed region with interrogation windows of 16×16 pixels. Using the velocity measurements, various turbulence characteristics (e.g., the mean and the root mean square (r.m.s.) velocities, two-point correlation functions and an integral scale of turbulence) have been obtained in our experiments. In particular, we determine the mean and r.m.s. velocities for every point of a velocity map by averaging over 530 independent maps. We obtain also the integral length scales of turbulence ℓ_y and ℓ_z in the horizontal Y and the vertical Z directions from the two-point correlation functions of the velocity field.

Next, we obtain the particle spatial distribution by the PIV system using the effect of the Mie light scattering by particles [53]. To this end, we determine the mean inten-

sity of scattered light in 80×64 interrogation windows with the size 16×16 pixels. This allows us to find the vertical distribution of the intensity of the scattered light in 80 vertical strips composed of 64 interrogation windows. In particular, we take into account that the light radiation energy flux scattered by small particles is given by $E_s \propto E_0 \Psi(\pi d_p / \lambda; a_0; n)$. Here Ψ is the scattering function, d_p is the particle diameter, λ is the wavelength, a_0 is the index of refraction. The energy flux incident at the particle is given by $E_0 \propto \pi d_p^2 / 4$. Note that when $\lambda > \pi d_p$, the scattering function Ψ is determined by the Rayleigh's law, $\Psi \propto d_p^4$. In opposite case for small λ , the scattering function Ψ is independent of the particle diameter and the wavelength. In a general case, the scattering function Ψ is determined by the Mie equations [54].

Finally, we take into account that the light radiation energy flux scattered by small particles is $E_s \propto E_0 n (\pi d_p^2 / 4)$. This implies that the scattered light energy flux incident on the charge-coupled device (CCD) camera probe is proportional to the particle number density n . The ratio of the scattered radiation fluxes at two locations in the flow and at the image measured with the CCD camera is equal to the ratio of the particle number densities at these two locations. For the normalization of the scattered light intensity E^T obtained in a temperature-stratified turbulence, we use the distribution of the scattered light intensity E measured in the isothermal case obtained under the same conditions. Indeed, as follows from our measurements applying different concentrations of the incense smoke, the distribution of the scattered light intensity averaged over a vertical coordinate is independent of the particle number density in the isothermal flow. Therefore, using this normalization, we can characterize the spatial distribution of particle number density $n \propto E^T / E$ in the non-isothermal turbulence.

Note that the measurement technique and data processing procedure described in this section are similar to those used by us in various experiments with turbulent convection [36, 55, 56] and stably stratified turbulence [35, 57]. In addition, the similar measurement technique and data processing procedure in the experiments have been performed previously by us to investigate the phenomenon of turbulent thermal diffusion in a homogeneous turbulence [25, 31–33] as well as for study of small-scale particle clustering [58].

IV. EXPERIMENTAL RESULTS

In this section we discuss the obtained experimental results in a forced convective turbulence with one oscillating grid in the air flow. There are two sources of turbulence in a forced convective turbulence with heated bottom wall of the chamber and cooling upper wall. In particular, the turbulent kinetic energy is increased by buoyancy and the grid oscillations. In our experiments, the frequency f of the grid oscillations is $f = 10.5$ Hz,

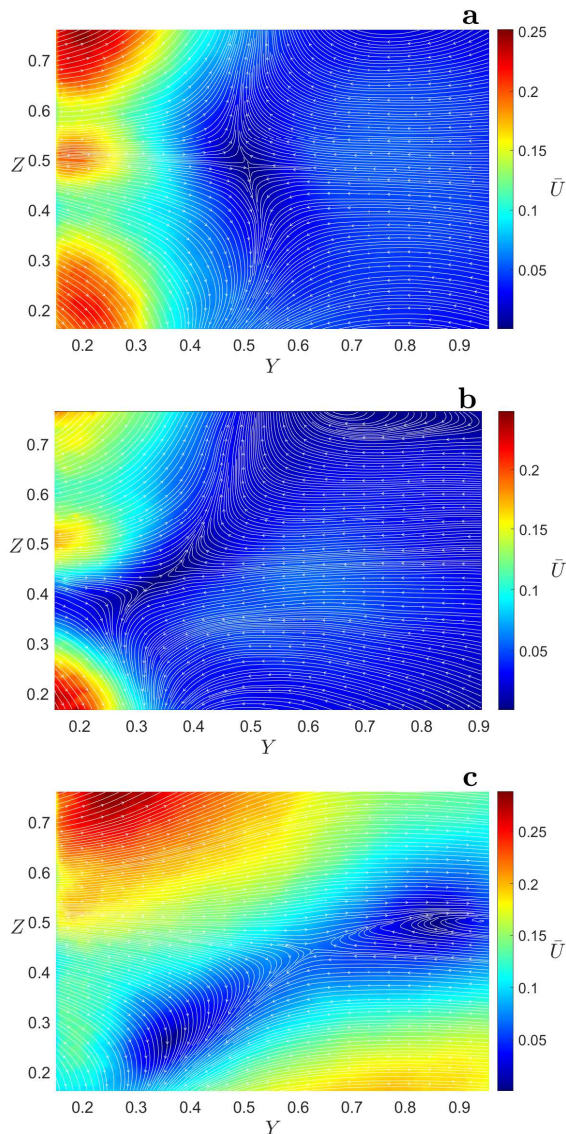


FIG. 2. Mean velocity field in the core flow for (a) isothermal turbulence; (c) stably stratified turbulence; (b) forced convective turbulence. The velocity is measured in m/s and coordinates Y and Z are normalized by $L_z = 26$ cm.

which yields the maximum turbulence intensity in our experimental set-up.

Note that early laboratory experiments [59–65] which have been conducted in isothermal turbulence with one oscillating grid in a water flow have demonstrated that the r.m.s. velocity behaves as $\sqrt{\langle \mathbf{u}'^2 \rangle} \propto f Y^{-1}$, while the integral turbulence length scale increases linearly with the distance Y from a grid. Therefore, the fluid Reynolds numbers as well as the turbulent diffusion coefficient of particles are nearly independent of the distance Y from the grid. Our previous [35] and present studies in turbulence with one oscillating grid confirm these findings.

In the present study we conduct experiments in a forced convective turbulence with one oscillating grid for

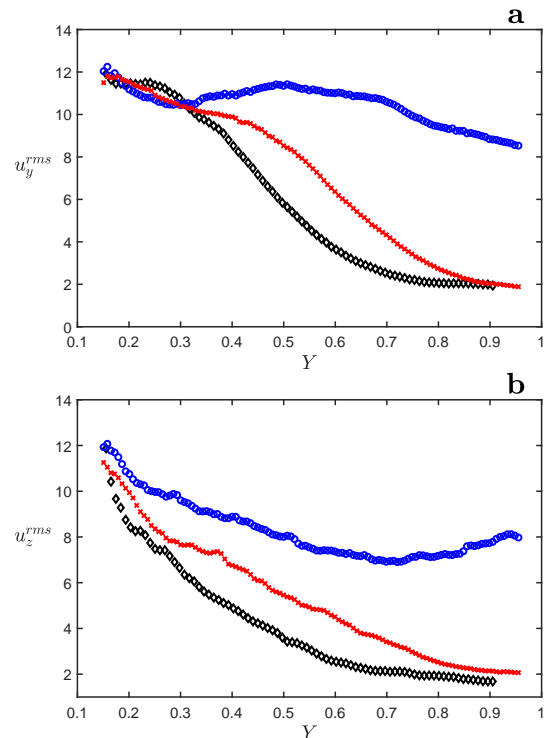


FIG. 3. Horizontal $u_y^{(rms)}$ (upper panel) and vertical $u_z^{(rms)}$ (lower panel) components of the turbulent velocity versus normalized coordinate Y averaged over the vertical coordinate Z for isothermal turbulence (red); stably stratified turbulence (black) and forced convective turbulence (blue). The velocity is measured in cm/s and Y is normalized by $L_z = 26$ cm.

the temperature difference $\Delta T = 50$ K between the bottom and top walls of the chamber. Using the PIV system we measure velocity field in the chamber for an isothermal and a forced convective turbulence, which allows us to determine various turbulence characteristics. In particular, we obtain the spatial distributions of the mean velocity in convective turbulence with large-scale circulations, the vertical and horizontal profiles of the r.m.s turbulent velocity and the integral turbulence length scales. Since the oscillating grid is located near by the left wall of the chamber, and the amplitude of the grid oscillations is 6 cm, we measure velocity field in the horizontal direction starting 20 cm away the left wall of the chamber. We compare these results with those obtained in our recent experiments [35] with stably stratified turbulence produced by one oscillating grid in the air flow.

Figure 2 with the mean velocity patterns \bar{U} in the main fluid flow for isothermal, stably stratified turbulence and convective turbulence, demonstrates that the temperature stratification and additional forcing strongly affect the mean velocity distributions. Contrary to our previous experiments with a forced convection with two oscillating grids [36], the large-scale circulations in the convective turbulence with one oscillating grid are not destroyed at the frequency 10.5 Hz of the grid oscillations, but their structure is strongly deformed (see the bottom panel in

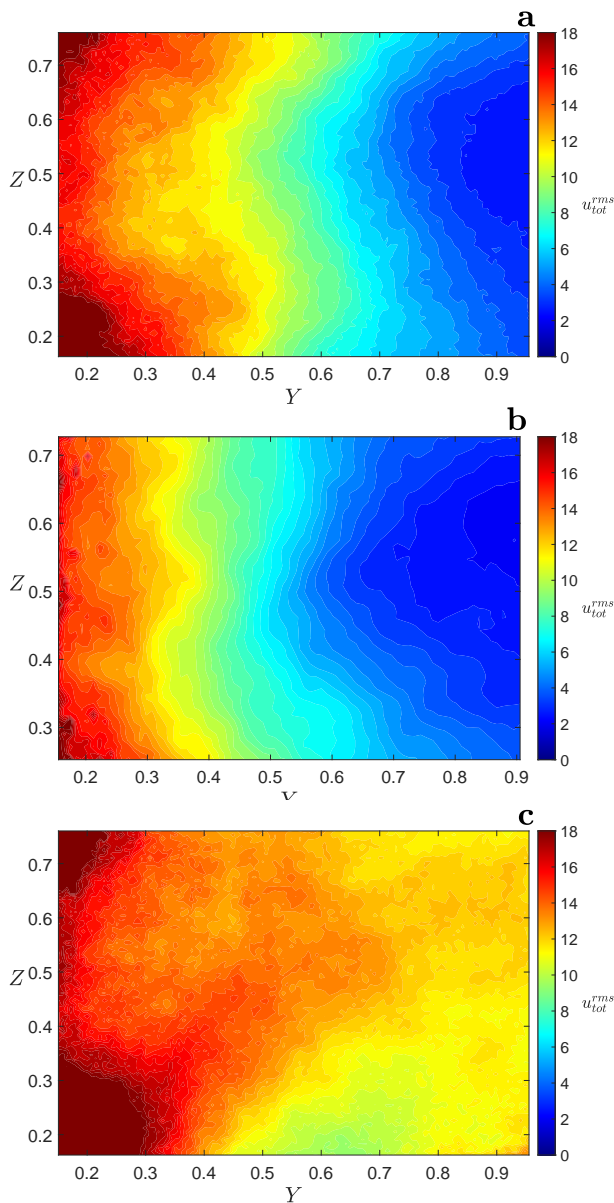


FIG. 4. Distributions of the turbulent velocity $u_{\text{tot}}^{(\text{rms})} = [\langle u_y^2 \rangle + \langle u_z^2 \rangle]^{1/2}$ for (a) isothermal turbulence; (b) stably stratified turbulence and (c) forced convective turbulence. The velocity is measured in cm/s and coordinates are normalized by $L_z = 26$ cm.

Fig. 2).

Similar effects of the temperature stratification and additional forcing are also seen in the horizontal profiles of velocity fluctuations (see Fig. 3, where we plot the horizontal $u_y^{(\text{rms})}$ and vertical $u_z^{(\text{rms})}$ components of turbulent velocities as the functions of Y averaged over the vertical coordinate Z for isothermal turbulence, stably stratified turbulence and convective turbulence). The turbulent velocities for convective turbulence are larger than for isothermal turbulence, while the turbulent velocities for stably stratified turbulence are smaller than those for

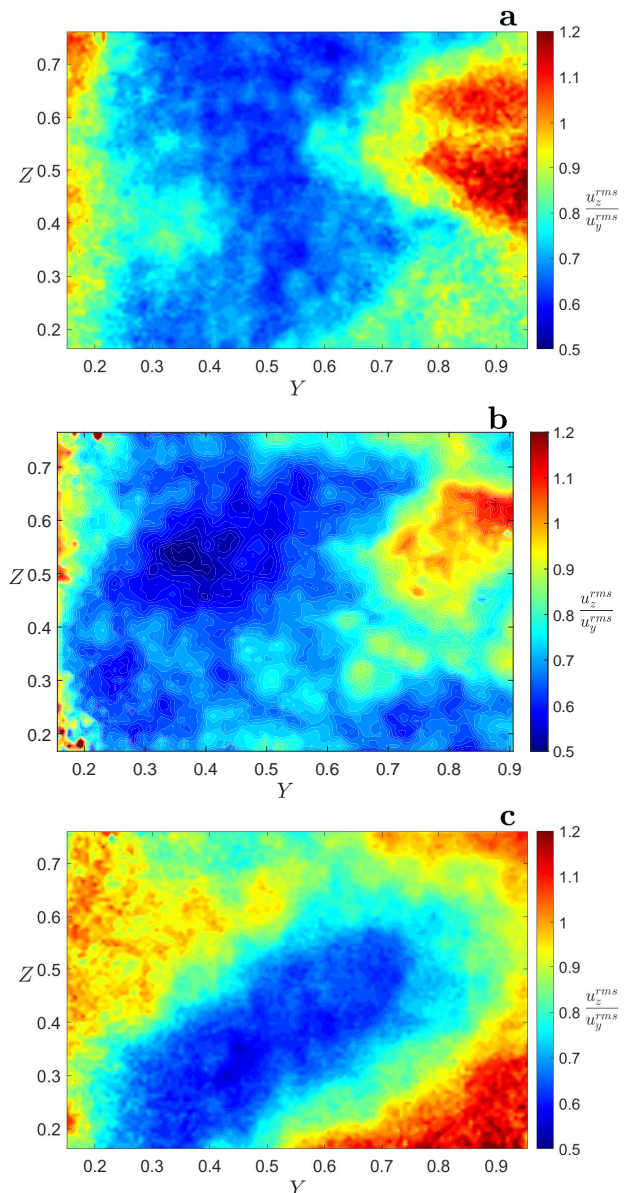


FIG. 5. Distributions of the anisotropy parameter $u_z^{(\text{rms})}/u_y^{(\text{rms})}$ of the turbulent velocity for (a) isothermal turbulence; (b) stably stratified turbulence and (c) forced convective turbulence. The velocity is measured in cm/s and coordinates are normalized by $L_z = 26$ cm.

isothermal and convective turbulence. This is because the buoyancy increases the turbulent kinetic energy for convective turbulence and decreases it for stably stratified turbulence.

The oscillating grid strongly affects convective turbulence, as can be seen in Figs. 4 and 5, where we show the distributions of the turbulent velocity $u_{\text{tot}}^{(\text{rms})} = [\langle u_y^2 \rangle + \langle u_z^2 \rangle]^{1/2}$ and the anisotropy parameter $u_z^{(\text{rms})}/u_y^{(\text{rms})}$ for the turbulent velocity components for isothermal, stably stratified and convective turbulence. Figure 5 demonstrates that the anisotropy for isothermal and stably

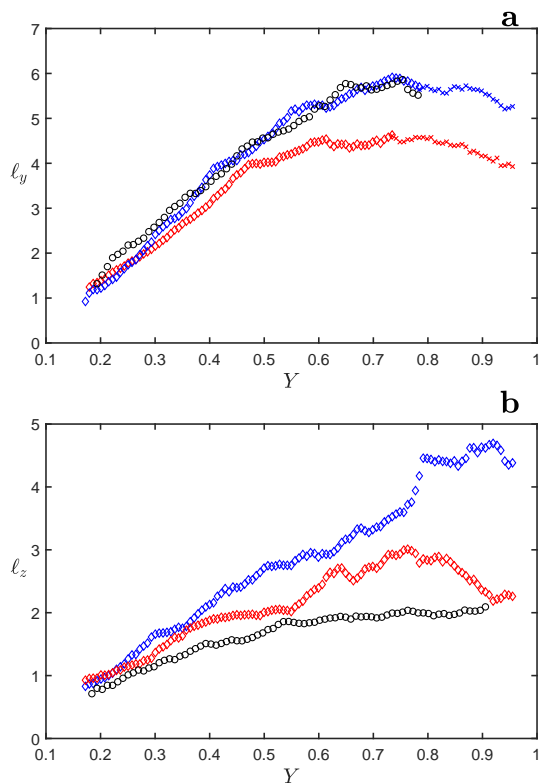


FIG. 6. Horizontal ℓ_y and vertical ℓ_z integral turbulent length scales versus normalized coordinate Y averaged over Z for isothermal turbulence (red); stably stratified turbulence (black) and forced convective turbulence (blue). The velocity is measured in cm/s and Y is normalized by $L_z = 26$ cm.

stratified turbulence is more stronger than that for convective turbulence. This is not surprising since the large-scale circulation enhances the mixing in the convective turbulence, and it results in decrease of the turbulence anisotropy parameter $u_z^{(\text{rms})}/u_y^{(\text{rms})}$. The same tendencies are also seen for the horizontal ℓ_y and vertical ℓ_z integral turbulent length scales shown in Fig. 6, as well as for the distributions of the anisotropy parameter ℓ_z/ℓ_y of the integral turbulent length scales (see Fig. 7).

To investigate the phenomenon of turbulent thermal diffusion in a forced convective turbulence, we measure the spatial distributions of the mean temperature and the mean particle number density. When small solid particles are injected into the chamber, their initial spatial distributions are nearly homogeneous. Due to the effective pumping velocity caused by a combined effect of temperature-stratified turbulence and particle inertia (described in terms of turbulent thermal diffusion) the final spatial distributions of the mean particle number density is expected to be strongly inhomogeneous.

Sedimentation of particles can also result in a formation of inhomogeneous particle distributions near the bottom wall of the chamber. However, this effect in our experiments is very weak, because the terminal fall velocity for the micron-size particles is about 10^{-2} cm/s,

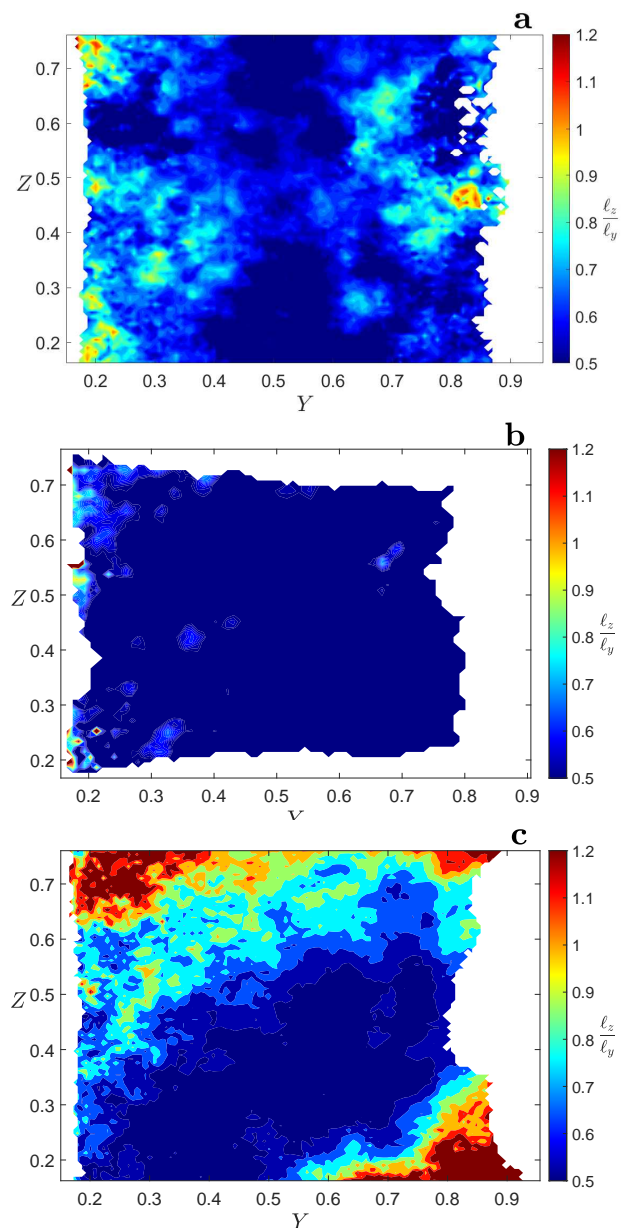


FIG. 7. Distributions of the anisotropy parameter ℓ_z/ℓ_y of the integral turbulent length scales for (a) isothermal turbulence; (b) stably stratified turbulence and (c) forced convective turbulence. The velocity is measured in cm/s and coordinates are normalized by $L_z = 26$ cm.

while the turbulent velocity in the experiments with the forced convective turbulence is much larger than the particle terminal fall velocity (it is about 18 cm/s near the grid and is more than 12 cm/s far from the grid). On the other hand, our estimates for the effective pumping velocity due to turbulent thermal diffusion shows that it is more than 3 – 5 cm/s near the grid and is about 0.5 cm/s far from the grid. Note also that the Stokes time for the micron-size particles is about 1.5×10^{-6} s, while in the forced convective turbulence the Kolmogorov time

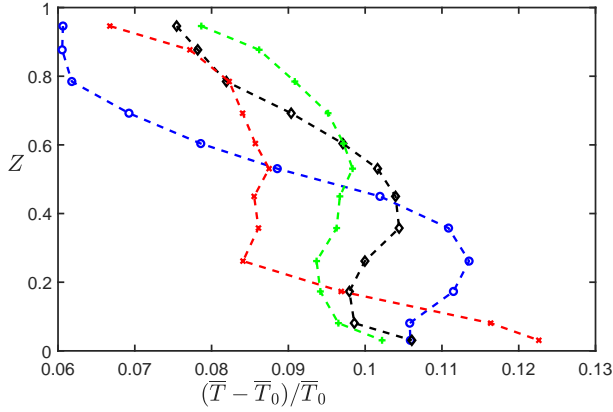


FIG. 8. Vertical profiles of the relative normalized mean temperature $(\bar{T} - \bar{T}_0)/\bar{T}_0$ in the forced convective turbulence averaged over different horizontal regions: $Y = 4 - 10$ cm (blue, circles); $Y = 11 - 16$ cm (black, diamond); $Y = 17 - 25$ cm (green, crosses) and $Y = 24.5 - 28.5$ cm (red, slanting crosses), where Z is normalized by $L_z = 26$ cm.

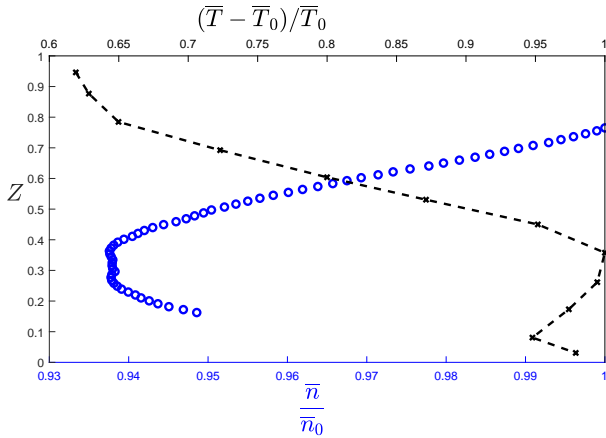


FIG. 9. Vertical profiles of the relative normalized mean temperature $(\bar{T} - \bar{T}_0)/\bar{T}_0$ (black, crosses) and the normalized mean particle number density $\bar{n}(Y, Z)/\bar{n}_0$ (blue, circles) in the forced convective turbulence averaged over horizontal region $Y = 4 - 15$ cm (near the grid). The coordinate Z is normalized by $L_z = 26$ cm.

varies from 7×10^{-3} s near the grid up to 4×10^{-3} s far from the grid. Therefore, the turbulent and effective pumping velocities in our experiments are much larger than the terminal fall velocity for micron-size particles.

Our experiments with a forced convective turbulence with large-scale circulations show that the mean temperature is strongly nonuniform. In particular, as follows from Fig. 8 (where we plot vertical profiles of the relative normalized mean temperature $(\bar{T} - \bar{T}_0)/\bar{T}_0$ averaged over different horizontal regions), the normalized mean temperature near the grid increases with the height Z , reaches the maximum and decreases nearly linearly with the height Z , where \bar{T}_0 is the reference mean temperature. Far from the grid, the behavior of the mean temperature is even more complicated, e.g., the normalized

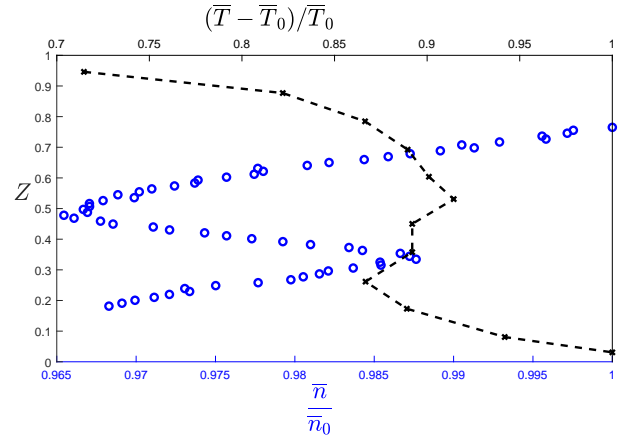


FIG. 10. Vertical profiles of the relative normalized mean temperature $(\bar{T} - \bar{T}_0)/\bar{T}_0$ (black, crosses) and the normalized mean particle number density $\bar{n}(Y, Z)/\bar{n}_0$ (blue, circles) in the forced convective turbulence averaged over horizontal region $Y = 17 - 24$ cm (far from the grid). The coordinate Z is normalized by $L_z = 26$ cm.

mean temperature $(\bar{T} - \bar{T}_0)/\bar{T}_0$ decreases with the height Z , reaches the minimum and increases with the height Z reaching the maximum, and finally it decreases nearly linearly with the height Z (see Fig. 8).

To demonstrate the phenomenon of turbulent thermal diffusion in the forced convective turbulence, we show in Figs. 9 and 10 the vertical profiles of the relative normalized mean temperature $(\bar{T} - \bar{T}_0)/\bar{T}_0$ (black crosses) and the normalized mean particle number density $\bar{n}(Y, Z)/\bar{n}_0$ (blue circles) near the grid (see Figs. 9) and far from the grid (see Figs. 10). Due to the phenomenon of turbulent thermal diffusion, the behaviour of the normalized mean particle number density is opposite to the normalized mean temperature, i.e., the mean particle number density increases in the regions where the mean temperature decreases, and the mean particle number density reaches the maximum at the minimum of the mean temperature, and vice versa. Therefore, Figs. 9 and 10 clearly demonstrate that particles are accumulated in the vicinity of the minimum of the mean temperature even in very complicated temperature field.

In the stably stratified turbulence, the behaviour of the mean temperature and the mean particle number density is more simple than for the forced convective turbulence [35]. In particular, the mean temperature increases linearly with the height Z in the flow for the stably stratified turbulence, and the mean particle number density decreases linearly with the height Z due to the phenomenon of turbulent thermal diffusion.

To determine the effective turbulent thermal diffusion coefficient α for particles in the forced inhomogeneous and anisotropic convective turbulence, we show in Fig. 11 the normalized mean particle number density \bar{n}/\bar{n}_0 as the function of the relative normalized mean temperature $(\bar{T} - \bar{T}_0)/\bar{T}_0$, where the slope of this dependence yields the coefficient α . In particular, we use a solution (26)

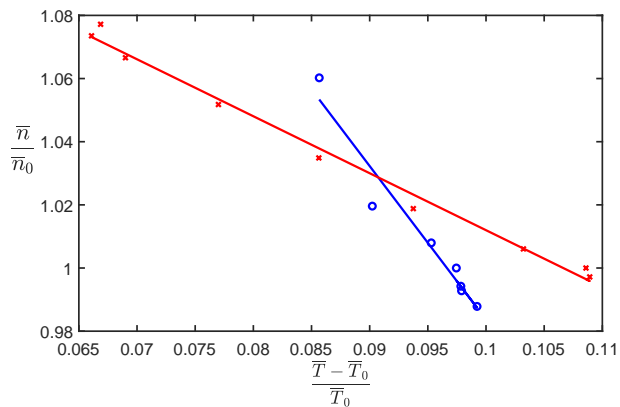


FIG. 11. The normalized mean particle number density \bar{n}/\bar{n}_0 versus the relative normalized mean temperature $(\bar{T}-\bar{T}_0)/\bar{T}_0$ averaged over different horizontal regions: $Y = 4 - 15$ cm (blue, circles) with $\alpha = 4.86$ and $Y = 16 - 24$ cm (red, crosses) with $\alpha = 1.74$ in the forced convective turbulence.

for Eq. (25) for the mean particle number density \bar{n} written in a steady-state, where we assume that $D_T \gg D$ and neglect small terminal fall velocity. Thus, we arrive at the following expression $\bar{n}/\bar{n}_0 = 1 - \alpha(\bar{T} - \bar{T}_0)/\bar{T}_0$, which shows that the effective turbulent thermal diffusion coefficient α for particles in the forced convective turbulence is $\alpha = 4.86$ for particles accumulated in the regions $Y = 4 - 15$ cm, and $\alpha = 1.74$ for particles accumulated in the regions $Y = 16 - 24$ cm (see Fig. 11). Now we take into account that turbulence far from the grid is less stronger than that near the grid. Therefore, the effective turbulent thermal diffusion coefficient α near the grid is larger than that far from the grid. Therefore, this experimental study has demonstrated the effect of turbulent thermal diffusion in an inhomogeneous and anisotropic forced convective turbulence.

V. CONCLUSIONS

In the present study, the effect of turbulent thermal diffusion of small solid particles, resulting in formation of large-scale inhomogeneities in particle spatial distributions in a temperature-stratified turbulence, has been investigated experimentally for micron-size particles in an inhomogeneous convective turbulence forced by one oscillating grid in the air flow. The obtained experimental results have been compared with the results of our previous experiments [35, 36] conducted in an inhomogeneous and anisotropic stably stratified turbulence [35] produced by a one oscillating grid and in a forced con-

vection with two oscillating grids in the air flow [36]. We have found that contrary to our previous experiments with a forced convection with two oscillating grids [36], the large-scale circulations in the convective turbulence with a one oscillating grid are not destroyed at the maximum frequency 10.5 Hz of the grid oscillations, but their structure is deformed (see Fig. 2). The measured vertical turbulent velocities for convective turbulence are stronger than for both, isothermal turbulence and stably stratified turbulence produced by a one oscillating grid, since the buoyancy increases the turbulent kinetic energy for convective turbulence and decreases it for stably stratified turbulence. These effects are also observed in the measured vertical integral turbulent length scales obtained from the two-point correlation functions for velocity fluctuations.

To study phenomenon of turbulent thermal diffusion, we measure spatial distributions of the mean temperature and mean particle number density in many locations. We have found that in the convective turbulence near the grid, the mean temperature increases with the height reaching the maximum and then it decreases nearly linearly with the increase of the height. On the other hand, far from the grid the behavior of the mean temperature in the convective turbulence is more complicated. The mean fluid temperature decreases with the height reaching the minimum, and for larger heights it increases with the height reaching the maximum, and finally it decreases nearly linearly with the height (see Fig. 8).

The behaviour of the mean particle number density is opposite to the mean temperature. In particular, the mean particle number density increases in the regions where the mean temperature decreases, reaching the maximum near by the minimum of the mean temperature (see Figs. 9 and 10). This implies that our experiments in convective and stably stratified turbulence with micron-size solid particles have clearly demonstrated the existence of the phenomenon of turbulent thermal diffusion, which causes particle accumulation in the vicinity of the minimum of the mean temperature even in a complicated vertical profile of the mean fluid temperature. We have determined the effective turbulent thermal diffusion coefficient using the vertical profiles of the mean temperature and the mean particle number density. We also have demonstrated that the obtained experimental results are in agreement with the theoretical predictions.

DATA AVAILABILITY

The data that support the findings of this study are available from the corresponding author upon reasonable request.

-
- [1] G. T. Csanady, *Turbulent Diffusion in the Environment* (Reidel, Dordrecht, 1980).
 [2] Ya. B. Zeldovich, A. A. Ruzmaikin, and D. D. Sokoloff,

The Almighty Chance (Word Scientific Publ., Singapore, 1990).

- [3] A. K. Blackadar, *Turbulence and Diffusion in the Atmo-*

- sphere* (Springer, Berlin, 1997).
- [4] J. H. Seinfeld and S. N. Pandis, *Atmospheric Chemistry and Physics. From Air Pollution to Climate Change.*, 2nd ed. (John Wiley & Sons, NY, 2006).
 - [5] L. I. Zaichik, V. M. Alipchenkov, and E. G. Sinaiski, *Particles in turbulent flows* (John Wiley & Sons, NY, 2008).
 - [6] C. T. Crowe, J. D. Schwarzkopf, M. Sommerfeld and Y. Tsuji, *Multiphase flows with droplets and particles*, second edition (CRC Press LLC, NY, 2011).
 - [7] I. Rogachevskii, *Introduction to Turbulent Transport of Particles, Temperature and Magnetic Fields* (Cambridge University Press, Cambridge, 2021).
 - [8] M. Caporali, F. Tampieri, F. Trombetti and O. Vittori, Transfer of particles in nonisotropic air turbulence, *J. Atmosph. Sci.* **32**, 565 (1975).
 - [9] M. Reeks, The transport of discrete particle in inhomogeneous turbulence, *J. Aerosol Sci.* **14**, 729 (1983).
 - [10] A. Guha, A unified Eulerian theory of turbulent deposition to smooth and rough surfaces, *J. Aerosol Sci.* **28**, 1517 (1997).
 - [11] T. Elperin, N. Kleeorin and I. Rogachevskii, Formation of inhomogeneities in two-phase low-Mach-number compressible turbulent fluid flows, *Int. J. Multiphase Flow* **24**, 1163 (1998).
 - [12] A. Guha, Transport and deposition of particles in turbulent and laminar flow, *Annu. Rev. Fluid Mech.* **40**, 311 (2008).
 - [13] Dh. Mitra, N. E. L. Haugen and I. Rogachevskii, Turbophoresis in forced inhomogeneous turbulence, *Europ. Phys. J. Plus* **133**, 35 (2018).
 - [14] F. De Lillo, M. Cencini, S. Musacchio and G. Boffetta, Clustering and turbophoresis in a shear flow without walls. *Phys. Fluids* **28**, 035104 (2016).
 - [15] G. Sardina, P. Schlatter, L. Brandt, F. Picano, and C. M. Casciola, Wall accumulation and spatial localization in particle-laden wall flows. *J. Fluid Mech.* **699**, 50-78 (2012).
 - [16] D. Kaftory, G. Hetsroni, and S. Banerjee, Particle behaviour in the turbulent boundary layer. I. Motion, deposition, and entrainment. *Phys. Fluids* **7**, 1095-1106 (1995).
 - [17] M. Righetti and G. P. Romano, 2004. Particle-fluid interactions in a plane near-wall turbulent flow. *J. Fluid Mech.* **505**, 93 (2004).
 - [18] T. Elperin, N. Kleeorin and I. Rogachevskii, Turbulent thermal diffusion of small inertial particles, *Phys. Rev. Lett.* **76**, 224 (1996).
 - [19] T. Elperin, N. Kleeorin and I. Rogachevskii, Turbulent barodiffusion, turbulent thermal diffusion and large-scale instability in gases, *Phys. Rev. E* **55**, 2713 (1997).
 - [20] T. Elperin, N. Kleeorin and I. Rogachevskii, Mechanisms of formation of aerosol and gaseous inhomogeneities in the turbulent atmosphere, *Atmosph. Res.* **53**, 117 (2000).
 - [21] T. Elperin, N. Kleeorin, I. Rogachevskii and D. Sokoloff, Passive scalar transport in a random flow with a finite renewal time: Mean-field equations, *Phys. Rev. E* **61**, 2617 (2000).
 - [22] T. Elperin, N. Kleeorin, I. Rogachevskii and D. Sokoloff, Mean-field theory for a passive scalar advected by a turbulent velocity field with a random renewal time, *Phys. Rev. E* **64**, 026304 (2001).
 - [23] R. V. R. Pandya and F. Mashayek, Turbulent thermal diffusion and barodiffusion of passive scalar and dispersed phase of particles in turbulent flows, *Phys. Rev. Lett.* **88**, 044501 (2002).
 - [24] M. W. Reeks, On model equations for particle dispersion in inhomogeneous turbulence, *Int. J. Multiph. Flow* **31**, 93 (2005).
 - [25] G. Amir, N. Bar, A. Eidelman, T. Elperin, N. Kleeorin and I. Rogachevskii, Turbulent thermal diffusion in strongly stratified turbulence: Theory and experiments, *Phys. Rev. Fluids* **2**, 064605 (2017).
 - [26] N. E. L. Haugen, N. Kleeorin, I. Rogachevskii and A. Brandenburg, Detection of turbulent thermal diffusion of particles in numerical simulations, *Phys. Fluids* **24**, 075106 (2012).
 - [27] I. Rogachevskii, N. Kleeorin and A. Brandenburg, Compressibility in turbulent magnetohydrodynamics and passive scalar transport: mean-field theory, *J. Plasma Phys.* **84**, 735840502 (2018).
 - [28] M. Sofiev, V. Sofieva, T. Elperin, N. Kleeorin, I. Rogachevskii and S. S. Zilitinkevich, Turbulent diffusion and turbulent thermal diffusion of aerosols in stratified atmospheric flows, *J. Geophys. Res.* **114**, D18209 (2009).
 - [29] T. Elperin, N. Kleeorin, Podolak, M., and I. Rogachevskii, A mechanism for the formation of aerosol concentrations in the atmosphere of Titan, *Planetary and Space Science* **45**, 923-929 (1997).
 - [30] A. Hubbard, Turbulent thermal diffusion: a way to concentrate dust in protoplanetary discs, *Monthly Notes Roy. Astron. Soc.* **456**, 3079-3089 (2016).
 - [31] J. Buchholz, A. Eidelman, T. Elperin, G. Grünefeld, N. Kleeorin, A. Krein, I. Rogachevskii, Experimental study of turbulent thermal diffusion in oscillating grids turbulence, *Experim. Fluids* **36**, 879 (2004).
 - [32] A. Eidelman, T. Elperin, N. Kleeorin, A. Krein, I. Rogachevskii, J. Buchholz, and G. Grünefeld, Turbulent thermal diffusion of aerosols in geophysics and in laboratory experiments, *Nonl. Proc. Geophys.* **11**, 343 (2004).
 - [33] A. Eidelman, T. Elperin, N. Kleeorin, A. Markovich, I. Rogachevskii, Experimental detection of turbulent thermal diffusion of aerosols in non-isothermal flows, *Nonl. Proc. Geophys.* **13**, 109 (2006).
 - [34] A. Eidelman, T. Elperin, N. Kleeorin, I. Rogachevskii and I. Sapir-Katiraie, Turbulent thermal diffusion in a multi-fan turbulence generator with the imposed mean temperature gradient, *Experim. Fluids* **40**, 744 (2006).
 - [35] E. Elmakies, O. Schildkrot, N. Kleeorin, A. Levy, I. Rogachevskii, A. Eidelman, Experimental study of turbulent thermal diffusion of particles in inhomogeneous and anisotropic turbulence, *Phys. Fluids* **34**, 055125 (2022).
 - [36] M. Bukai, A. Eidelman, T. Elperin, N. Kleeorin, I. Rogachevskii and I. Sapir-Katiraie, Transition phenomena in unstably stratified turbulent flows, *Phys. Rev. E* **83**, 036302 (2011).
 - [37] S. A. Orszag, Analytical theories of turbulence, *J. Fluid Mech.* **41**, 363 (1970).
 - [38] A. Pouquet, U. Frisch, and J. Leorat, Strong MHD helical turbulence and the nonlinear dynamo effect, *J. Fluid Mech.* **77**, 321 (1976).
 - [39] P. H. Roberts and A. M. Soward, A unified approach to mean field electrodynamics, *Astron. Nachr.* **296**, 49 (1975).
 - [40] A. Brandenburg and K. Subramanian, Minimal tau approximation and simulations of the alpha effect, *Astron. Astrophys.* **439**, 835 (2005).
 - [41] A. Brandenburg, K.-H. Rädler, M. Rheinhardt, P. J.

- Käpylä, Magnetic diffusivity tensor and dynamo effects in rotating and shearing turbulence, *Astrophys. J.* **676**, 740 (2008).
- [42] I. Rogachevskii, N. Kleeorin, P. J. Käpylä, A. Brandenburg, Pumping velocity in homogeneous helical turbulence with shear, *Phys. Rev. E* **84**, 056314 (2011).
- [43] A. Brandenburg, K.-H. Rädler, and K. Kemel, Mean-field transport in stratified and/or rotating turbulence, *Astron. Astrophys.* **539**, A35 (2012).
- [44] T. Elperin, N. Kleeorin, M. Liberman, A. N. Lipatnikov, I. Rogachevskii, R. Yu, Turbulent diffusion of chemically reacting flows: Theory and numerical simulations, *Phys. Rev. E* **96**, 053111 (2017).
- [45] G. I. Taylor, Diffusion by continuous movements, *Proc. London Math. Soc.* **2**, No. 1, 196-212 (1922).
- [46] D. Enskog, 1911. Bemerkungen zu einer Fundamentalgleichung in der kinetischen Gastheorie. *Physik. Zs. Leipzig* **12**, 533-539 (1911).
- [47] D. Enskog, 1912. Zur Elektronentheorie der Dispersion und Absorption der Metalle. *Annalen der Physik* **343**, 731-763 (1912).
- [48] S. Chapman, The kinetic theory of a gas constituted of spherically symmetrical molecules. *Phil. Trans. Roy. Soc. London A* **211**, 433-483 (1912).
- [49] M. R. Maxey, The gravitational settling of aerosol particles in homogeneous turbulence and random flow field, *J. Fluid Mech.* **174**, 441 (1987).
- [50] R. J. Adrian, Particle-imaging techniques for experimental fluid mechanics, *Annu. Rev. Fluid Mech.* **23**, 261 (1991).
- [51] M. Raffel, C. Willert, S. Werely and J. Kompenhans, *Particle Image Velocimetry* (Springer, Berlin-Heidelberg, 2007).
- [52] J. Westerweel, Theoretical analysis of the measurement precision in particle image velocimetry, *Experim. Fluids* **29**, S3 (2000).
- [53] P. Guibert, M. Durget and M. Murat, Concentration fields in a confined two-gas mixture and engine in cylinder flow: laser tomography measurements by Mie scattering, *Experim. Fluids* **31**, 630-642 (2001).
- [54] C. F. Bohren and D. R. Huffman, *Absorption and Scattering of Light by Small Particles* (John Wiley and Sons, New York, 1983).
- [55] M. Bukai, A. Eidelman, T. Elperin, N. Kleeorin, I. Rogachevskii and I. Sapir-Katiraie, Effect of large-scale coherent structures on turbulent convection, *Phys. Rev. E* **79**, 066302 (2009).
- [56] I. Shimberg, O. Shriki, O. Shildkrot, N. Kleeorin, A. Levy, I. Rogachevskii, Experimental study of turbulent transport of nanoparticles in convective turbulence, *Phys. Fluids* **34**, 055126 (2022).
- [57] A. Eidelman, T. Elperin, I. Gluzman, N. Kleeorin and I. Rogachevskii, Experimental study of temperature fluctuations in forced stably stratified turbulent flows, *Phys. Fluids* **25**, 015111 (2013).
- [58] A. Eidelman, T. Elperin, N. Kleeorin, B. Melnik and I. Rogachevskii, Tangling clustering of inertial particles in stably stratified turbulence, *Phys. Rev. E* **81**, 056313 (2010).
- [59] J. S. Turner, The influence of molecular diffusivity on turbulent entrainment across a density interface, *J. Fluid Mech.* **33**, 639-656 (1968).
- [60] Turner, S. T., *Buoyancy Effects in Fluids* (Cambridge Univ. Press, Cambridge, 1973).
- [61] S. M. Thompson and J. S. Turner, Mixing across an interface due to turbulence generated by an oscillating grid, *J. Fluid Mech.* **67**, 349-368 (1975).
- [62] E. J. Hopfinger and J.-A. Toly, Spatially decaying turbulence and its relation to mixing across density interfaces, *J. Fluid Mech.* **78**, 155-175 (1976).
- [63] E. Kit, E. J. Strang and H. J. S. Fernando, Measurement of turbulence near shear-free density interfaces, *J. Fluid Mech.* **334**, 293-314 (1997).
- [64] M. A. Sánchez and J. M. Redondo, Observations from grid stirred turbulence, *Appl. Sci. Res.* **59**, 243-254 (1998).
- [65] P. Medina, M. A. Sánchez and J. M. Redondo, Grid stirred turbulence: applications to the initiation of sediment motion and lift-off studies, *Phys. Chem. Earth B* **26**, 299-304 (2001).